

On the relationship of energetic particle precipitation and mesopause temperature

Florine Enengl^{1,2,3,4}, Noora Partamies^{2,5}, Nickolay Ivchenko¹, and Lisa Baddeley^{2,5}

¹KTH Royal Institute of Technology, Stockholm, Sweden

²The University Centre in Svalbard, Norway

³ESA European Space Research and Technology Centre, The Netherlands

⁴University of Oslo, Norway

⁵Birkeland Centre for Space Science, Norway

Correspondence: Florine Enengl (florine@kth.se)

Abstract. Energetic Particle Precipitation (EPP) has the potential to change the neutral atmospheric temperature at the mesopause region. However, recent results are inconsistent leaving the mechanism and the actual effect still unresolved. Here we have searched for electron precipitation events and investigated a possible correlation between D region electron density enhancements and simultaneous neutral temperature changes. The rotational temperature of the excited hydroxyl (OH) molecules is retrieved from the spectrum of the OH airglow. The electron density is monitored by the EISCAT Svalbard Radar. [We use all available experiments](#) from the International Polar Year (IPY) in 2007–2008 until February 2019. Particle precipitation events are characterized by rapid increases in electron density by a factor of 4 at an altitude range of 80–95 km, which overlaps with the nominal altitude of the OH airglow layer. The OH airglow measurements and the electron density measurements are co-located. Most of our [8 10](#) electron precipitation events are associated with a temperature decrease of 10–20 K. [Two Four](#) events were related to temperature change less than 10 K. We interpret the results in terms of the change in the chemical composition in the mesosphere. Due to EPP ionisation the population of excited OH at the top of the airglow layer may decrease. As a consequence, the airglow peak height changes and the temperatures are probed at lower altitudes. The observed change in temperature thus depends on behaviour of the vertical temperature profile within the airglow layer. This is in agreement with conclusions of earlier studies, but is, for the first time, constructed from electron precipitation measurements as opposed to proxies. The EPP related temperature change recovers very fast, typically within less than 60 minutes. We therefore further conclude that this type of particle precipitation event would only have a significant impact on the longer-term heat balance in the mesosphere if the lifetime of the precipitation was much longer than that of a typical EPP event found in this study.

Copyright statement. TEXT

1 Introduction

20 Space weather phenomena can affect the dynamics and the heat balance of the atmosphere by depositing energy in the form of energetic particle precipitation. In particular, investigating the mesopause region (at 80–100 km), the boundary between the mesosphere and the thermosphere (Andrews, 2010), is important. At the lower boundary of the ionosphere and the upper boundary of the neutral atmosphere, the behaviour of neutral gas and ionized particles differ, which is why complex interactions between dynamics, photochemistry, heating and transport mechanisms take place and the atmospheric energy budget can be
25 altered.

Several studies have investigated the effects of energetic particle precipitation (EPP) on neutral temperatures in the mesopause region. Nesse Tyssøy et al. (2010) compared particle precipitation observed by NOAA POES satellites with neutral temperatures derived from the TIMED satellite. They used a dataset of 80 days within May–June and October–November in 2003 over the northern hemisphere. Temperature profiles were averaged over all local time hours for four flux levels of precipitating
30 energetic protons. A temperature increase of about 40 K was found at 115–120 km associated with strong fluxes of 80–250 keV protons in October–November. The strongest temperature increase of 15–20 K in May–June at the altitudes of 110–115 km was reported due to high fluxes of 30–80 keV protons. As particle precipitation events change the Pedersen conductivity, Joule heating may contribute to the increase in temperature at these altitudes. Further down in the atmosphere, at 85–90 km, only a minor cooling of 3–4 K during periods of high Kp values was observed due to precipitation of 250–800 keV protons (an
35 intense solar proton event).

The rotational hydroxyl (OH) airglow temperature was observed during six nights of the austral winter in 2008 by Suzuki et al. (2010b). These nights were selected to include high auroral activity and clear weather. In their study, the temperature was derived from spectra recorded at Syowa Station in Antarctica by a high-sensitivity spectrometer. During only one of these nights (27–28 March 2008), an increase in the temperature of 10 K over a time period of 15 minutes was observed. Furthermore,
40 a decrease in the relative intensity of the OH(8–4) Q branch of $\sim 23\%$ was found by comparing the pre-EPP level to that half an hour after the largest magnetic deflection. No such coherent behaviour was seen during the other nights. Suzuki et al. (2010b) suggested a relationship between EPP and the OH temperature based on measured disturbances in the horizontal magnetic field and variations in the cosmic radio noise absorption (CNA) over the course of several hours of activity. The average energy of the precipitating electrons during this night reached 10–20 keV. They discussed different mechanisms for causing the change
45 in the temperature. Joule heating was concluded to not contribute much, as the estimated heating rate required to explain the observed temperature increase at the mesopause height was three orders of magnitude higher than particle precipitation observations suggested. Direct particle heating, on the other hand, is produced by precipitating particles colliding with the atmospheric neutrals. This heating process is dependent on the incident particle energy and their deposition altitude. Similarly to the Joule heating, the authors estimated the energy deposition rate of EPP at the mesopause height, and concluded that the
50 high-energy particle flux required to explain the temperature change was unrealistically high. Atmospheric gravity waves were also excluded, as the intensity of the OH airglow and the rotational temperature did not show a positive correlation, which is characteristic for dynamics driven conditions, as described and modelled by Cho and Shepherd (2006). Suzuki et al. (2010b)

further discussed the possibility of a change in the height distribution of the OH airglow emission during auroral events. The initial profile of OH volume emission rates retrieved by the SABER instrument onboard the TIMED satellite was compared to an example of the disturbed layer. The comparison showed a decrease in the upper part of the disturbed layer as the thickness of the OH layer had decreased by 20%. If a change in the height distribution of the OH airglow emission occurred during an auroral event, an increase in temperature is not necessarily observed, as the outcome would depend on ~~the temperature gradient in the mesosphere~~ the local temperature in the mesosphere.

The connection between the geomagnetic activity and the long-term temperature at the mesopause region during solar cycles 23 and 24 was studied by Gavriljeva and Ammosov (2018). The OH rotational temperature was measured by the ground-based infrared spectrograph at Maimaga station (63°N, 129.5°E), and ascribed to an altitude of 87 km, which is commonly assumed to be the peak height of the OH layer. The seasonally averaged temperatures from 1999 to 2015 were included in the analysis. The results showed that the mesopause temperature from October to February is about 10 K higher during the years with high solar activity ($A_p > 8$) than during low activity years ($A_p \leq 8$). A solar activity dependence of OH airglow temperatures was also reported by Holmen et al. (2014). They concluded on a temperature change of about 4 K per 100 solar flux units (SFU) of the F10.7 radio flux. The question on the detailed relationship of EPP and the mesopause temperature was still left open.

The purpose of this study is to characterize the effects of the EPP on the mesopause temperature in more detail, using co-located measurements of precipitating electrons and the mesospheric temperature. The instrumentation is further described in section 2. Section 3 outlines the data used in this study, as well as the analysis of the EISCAT Svalbard Radar data. Finally, the results are shown and discussed in sections 4 and 5. The conclusions of the effects of the EPP on the mesopause temperature are summarized in section 6.

2 Instrumentation

Following Cresswell-Moorcock et al. (2013) we use the European Incoherent Scatter Scientific Association (EISCAT) radar data to identify electron precipitation events as electron density enhancements. Simultaneous and co-located neutral temperature measurements are determined using spectrometer measurements of the OH airglow. The derived rotational OH temperature is taken as the neutral temperature of the mesopause region, assuming that the excited OH molecules are in thermal equilibrium with the ambient atmosphere.

2.1 EISCAT Svalbard Radar

For this study the EISCAT Svalbard Radar (ESR, Wannberg et al. (1997)) in Longyearbyen, Norway (situated at a geographic latitude of 78.15°N and a geographic longitude of 16.02°E and at corrected geomagnetic coordinates of 75.43° and 110.68°) is used. The radar operates at the 500 MHz band and has a 32 m steerable parabolic dish antenna and a 42 m fixed parabolic antenna aligned to the local geomagnetic field. For our purpose, we searched for experiments with good height resolution at D region altitudes. The manda experiment (Tjulin, 2017) resolves altitudes of 80 to 100 km with 1–2 km height resolution and was therefore chosen for the radar campaigns in January and February 2019 for this study. In addition to manda, all previously

85 run `ipy` experiments were analyzed, as that experiment also covers the mesopause region with a vertical resolution of 4–5 km. The `manda` experiments utilize the 32 m dish and the `ipy` data are collected on the 42 m dish.

2.2 Ebert-Fastie airglow Spectrometer

The Ebert-Fastie spectrometer at the Kjell Henriksen Observatory (KHO) in Longyearbyen, Svalbard, is used to retrieve the winter temperature of the mesopause (Sigernes et al., 2003). The observatory is located only a kilometer away from the radar site, so it is practically co-located. The spectrometer scans the near infrared wavelength region from 824 to 871 nm which includes the rotational OH(6–2) band of the OH airglow. The spectrometer points to the zenith with a field-of-view of 5 degrees. It measures whenever the Sun is more than 12 degrees below the horizon, which at Svalbard latitudes (78.2°N) gives an optical observation season from the beginning of November until the end of February. The spectral resolution of the OH(6–2) band is 0.4 nm. One scan of the wavelength range takes 25 seconds but to obtain a good signal-to-noise ratio several scans are averaged during post-processing of the data. Most earlier studies use 1-hour averages. In this study, half-hour averaging is used for better temporal resolution. We further move the 30-min averaging window by 10-min time steps to obtain a smoothed temporal evolution of temperature. The rotational OH temperatures are obtained by fitting a synthetic spectrum to the measured band of emission lines. Using the intensities of four emission line pairs (P_1 & P_2) within the P branch of OH(6–2) the slope of the best fit determines the temperature. An oxygen auroral emission line at 844.6 nm lies in the middle of the OH(6–2) spectrum. The times when that emission intensity overtakes the OH emission intensity (fit covariance greater than 0.5) are excluded in the temperature analysis due an inaccurate fit. Other things causing poor fits and missing temperature values are cloudiness, high background illumination (e.g. scattered moonlight) or technical issues with the instrument. The threshold values for the fit variances have been determined empirically by viewing and fitting large datasets over decades. For consistency we have employed the same threshold values as in the earlier work (Sigernes et al., 2003; Holmen et al., 2013) at the event selection state. Once the events were selected, we relaxed the threshold values to obtain a more continuous data coverage. The covariance threshold was lowered to 0.2 as long as the fit variance criteria were still met. Similarly, the fit variance criterion for P_2 lines was lowered from 0.3 to 1.0 as long as the covariance (< 0.5) and P_1 line (< 0.05) criteria held. The uncertainties introduced by this procedure are reflected by the error bars in the displayed data. The accuracy of the fitting method in estimating rotational temperatures is ± 2 K. The error bars shown in this study represent the standard deviations (STD) over the averaged time, which are typically somewhat larger than the uncertainty of the method itself (see values in Table 1). In addition to the fitted temperature values, we use relative band brightness (non-calibrated arbitrary units) of the P branch of the OH(6–2) transition. These intensity values are routinely calculated and saved together with the rotational temperatures.

3 Data description and event selection

A total of 10220 hours of ESR data were initially inspected. The `ipy` and `manda` experiment contribute 10144 hours and 76 hours of data respectively. These experiments provide a sufficient height resolution to detect enhanced electron densities at the mesopause. Here the mesopause region is defined from an altitude of 80 to 100 km to include the hydroxyl (OH) peak height

at 76–90 km (Mulligan et al., 2009). Experiments run in field-aligned direction (42m: `ipy`, 32m: `manda`) or vertical pointing (32m: `manda`) are chosen. The data set starts at the International Polar Year 2007–2008 when the ESR was run continuously from 1 March 2007 to 29 February 2008 (Blelly et al., 2010). This year includes 8784 hours in the `ipy` experiment mode. 120 Additionally, all `manda` and `ipy` experiments from December, January and February every year until February 2019 are included in the analysis. The total of 1388 hours of ESR data between 2008–2019 were analyzed in more detail. Finally, the ESIRI experiment (ESR Ionospheric D-Region Experiment for Investigation of EPP) `manda` mode was run for a total of 48 hours in January (24 hours) and February 2019 (another 24 hours) to specifically collect data for this study. The experiment was run for six evenings between 16 to 22 UT (19 to 01 MLT).

125 The EISCAT raw data files (Auto-Correlation Functions (ACFs)) are analysed using the GUISDAP data package (Lehtinen and Huuskonen, 1996). This provides an iterative fitting of the ACFs and then, using a model ionosphere, produces the electron densities examined in this study. The post-integration time is 60 s. Data gaps are shown by white areas in the plots (Figures 1 and 2) and occur where GUISDAP has not managed to provide a fit. 10-minute averaged electron densities are calculated for the altitude ranges of 87–90 km and 91–94 km separately. The error of the electron density is averaged to give a mean error for 130 further analysis.

The search for the EPP events in the radar data is based on an earlier study by Cresswell-Moorcock et al. (2013). The onset is found by a sudden increase of the electron density (median value) by a factor of 5 over 5 minutes. For this study the electron density is averaged to 10 min resolution with an altitude resolution of 4 km. This criterion was slightly adapted to better suit the data from the two different EISCAT experiments. The previous study’s factor of 5 was attempted but since there were a 135 number of events just below this acceptance threshold the factor was adjusted to 4. We searched for an increase of electron density by a factor of 4 within 20 minutes from the precipitation onset. If onsets are found only 10 minutes apart, the latter onset is ignored.

The events are detected automatically but inspected and classified visually based on the temporal evolution of the electron density and the OH temperature. Events with large electron density errors of more than $5 \times 10^9 \text{ m}^{-3}$ are excluded. Events 140 which lack more than ~~a ± 3 hour analysis window from the event onset~~ one temperature measurement at or after the onset are also excluded. Events which show a particle precipitation signature of electron density enhancement through the whole ionospheric column (87–126 km) are sorted into the EPP category. Events which show an electron density enhancement limited to horizontal layer at the bottom of the E region (around 100 km) are categorized as sporadic E layers (Rapp et al., 2011). The remaining data not showing clear EPP or sporadic E layer behaviour are excluded from the analysis. The sporadic E layer 145 events are not discussed further in this paper. This selection results in a set of ~~eight~~ ten EPP events, which were categorized into groups of increasing, decreasing and stable (no change) temperature evolution over the EPP onset.

The electron density during the radar run on 6 January 2019 from 16:00 UT to 22:00 UT is shown in Figure 1 (top panel). The onset of the EPP is at 19:50 UT and the event lasted until 20:20 UT. The electron density at the lower part of the ionosphere during this experiment was low (mainly below 10^{10} m^{-3}) but abruptly increased at the EPP onset time. The OH rotational 150 temperature (middle panel) ~~experiences large variations (~ 20 K) during the hours leading to the precipitation onset when there is no electron density enhancements below 100 km altitude.~~ A small temperature dip (~ 5 K) is seen 10 minutes after the onset,

but the change is well within the measurement uncertainties and does not persist. The relative OH band brightness (bottom panel) minimised half an hour before the precipitation started and remained at that level until half an hour after the EEP onset. During this experiment the radar was pointed to zenith, which is aligned with the spectrometer field-of-view. The particle precipitation within the spectrometer field-of-view caused the oxygen auroral emission line to enhance so that one data point was missed in the temperature analysis.

4 Results

Our ten EPP events are listed in Table 1. The criterion for a ~~decreasing or increasing~~ changing mesopause temperature is that the change has to be larger than the standard deviation (STD) of the temperatures averaged over half an hour. An event is classified as stable (no change), if the temperature change from the value just before the onset to that 20 min after the onset time is within the STD of the averaged temperatures. As each of the data points is an average over the previous 30 minutes the point just prior to the onset is a representative for the temperature level before the precipitation starts, while the temperature value 20 minutes after the onset includes onset time information as well as any immediate changes after the onset. Apart from the eighth ninth and tenth event, all other events were measured by a field-aligned pointing radar experiment. Thus, the auroral emission does not obscure the temperature calculations as the two parameters were often measured side by side rather than in exactly the same column. The events associated with a temperature decrease (6 events) show a variable magnitude of the change from 10 to 40 degrees while events with a temperature increase (4 events) only undergo a few degrees' change and are thus classified as stable.

#	Event Date [UT]	T_{-2} [K]	T_{-1} [K]	T_0 [K]	T_{+1} [K]	T_{+2} [K]	ΔT [K]	classification
1	2007/12/29 23:30	225 ± 6			188 ± 16	185 ± 12	-40	decreasing
2	2008/02/28 02:50	227 ± 10	215 ± 21	187 ± 18	207 ± 6	202 ± 21	-13	decreasing
3	2013/12/06 21:50	224 ± 9	219 ± 3	212 ± 4	210 ± 0	196 ± 3	-23	decreasing
4	2014/01/21 15:20	229 ± 8	222 ± 2	214 ± 4	211 ± 4	212 ± 5	-10	decreasing
5	2014/01/24 02:10	212 ± 5	210 ± 5	198 ± 2	199 ± 3	198 ± 2	-12	decreasing
6	2014/01/24 15:20	218 ± 14	214 ± 9	212 ± 9	217 ± 7	217 ± 11	+3	stable
7	2014/01/25 02:40	228 ± 6	221 ± 4	224 ± 2	221 ± 5	224 ± 3	+3	stable
8	2016/02/06 19:50	194 ± 4	195 ± 7	187 ± 10	184 ± 6	182 ± 4	-13	decreasing
9	2019/01/05 21:50	202 ± 3	203 ± 8	198 ± 5	194 ± 7	210 ± 7	+7	stable
10	2019/01/06 19:50	196 ± 6	198 ± 3	192 ± 3	188 ± 5	199 ± 5	+1	stable

Table 1. Airglow temperature values (degrees in Kelvin in 30 min averages) before, at and after the event onsets for each EPP event. T_0 indicates the point closest to the event onset. The data points are ten minutes apart. For instance, T_{-1} refers to the data point 10 minutes before T_0 . All temperature values are accompanied with the 30-min STDs. The last columns indicate the observed change in the temperature over the EPP onset. The points compared in ΔT are T_{-1} to T_{+2} (as T_{-1} is not available for the first event T_{-2} used).

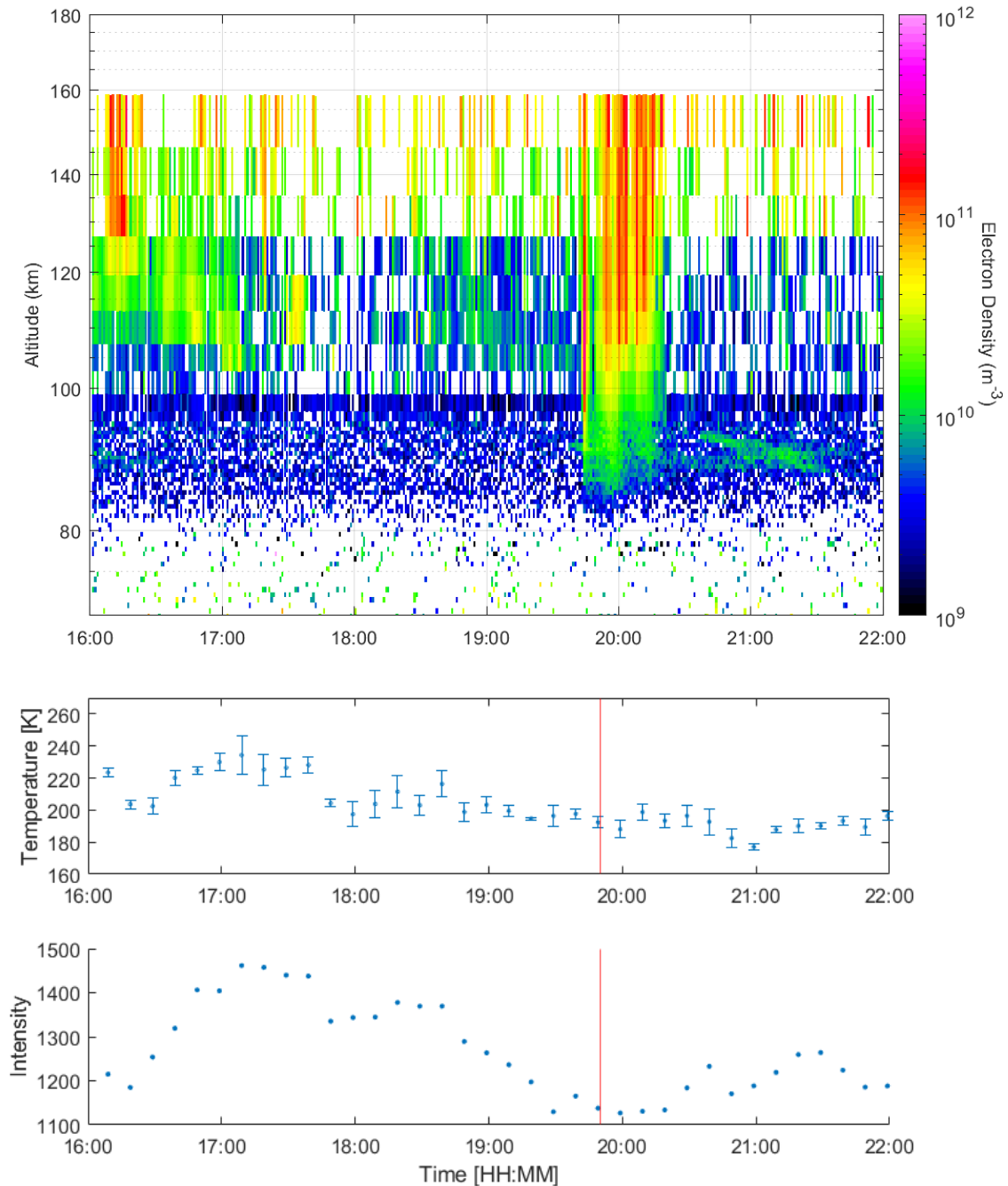
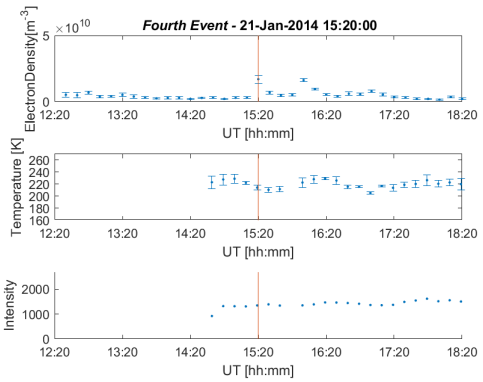
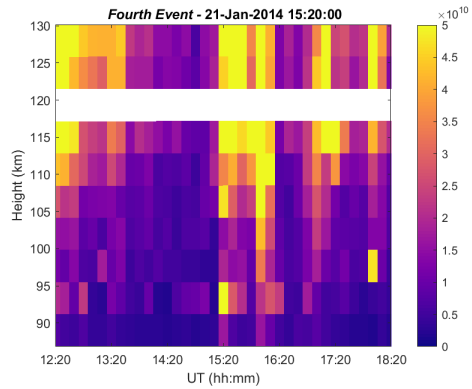
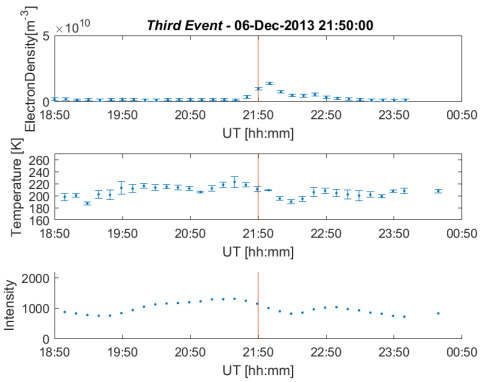
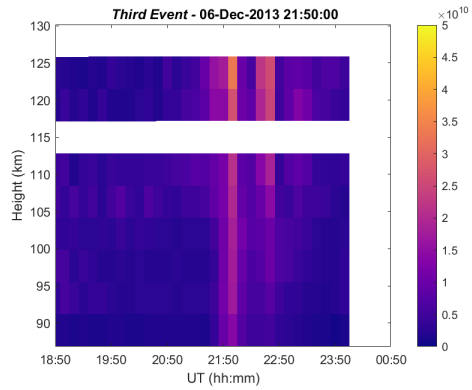
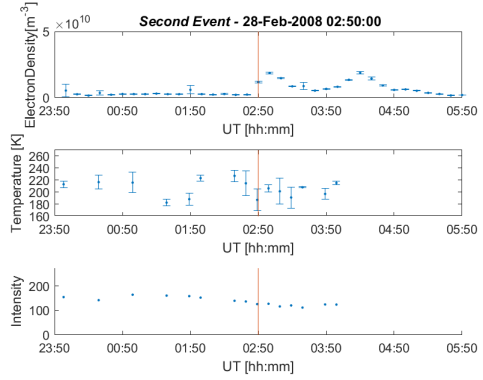
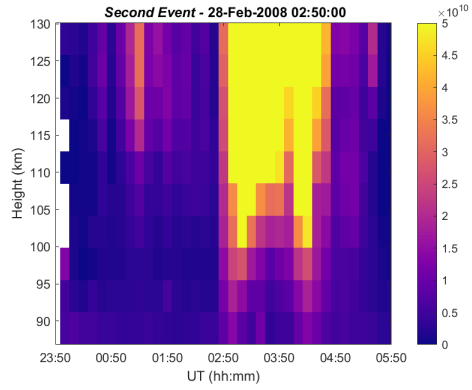
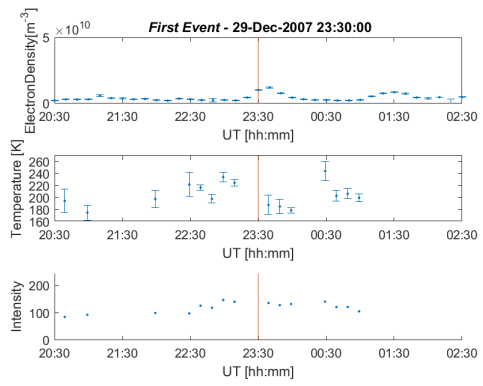
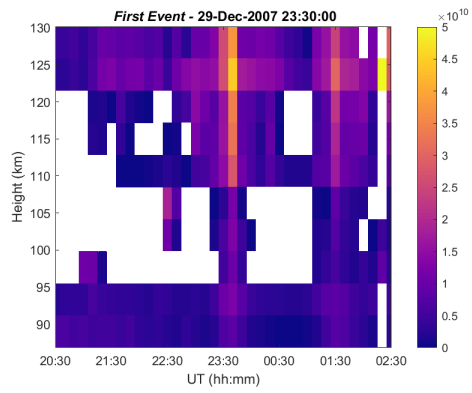
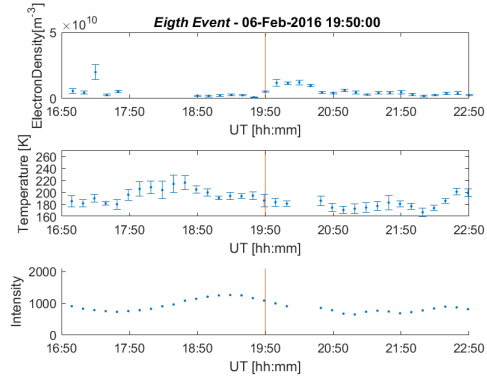
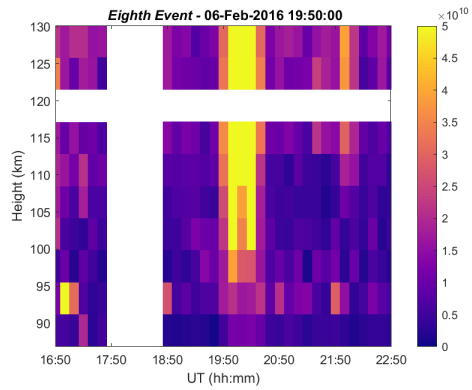
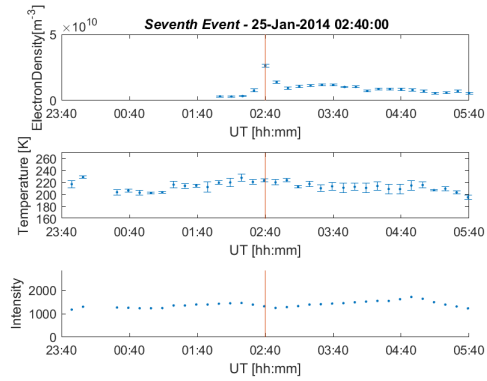
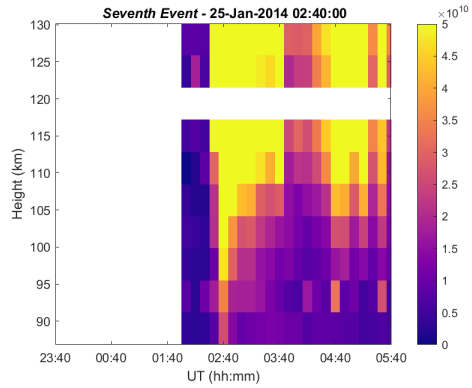
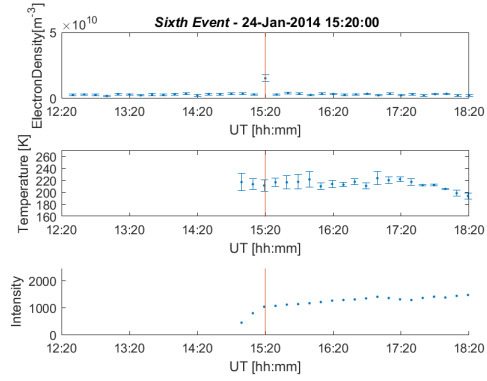
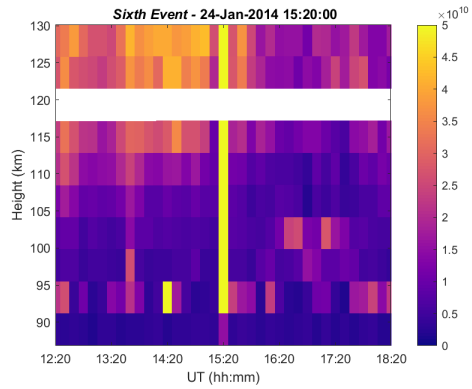
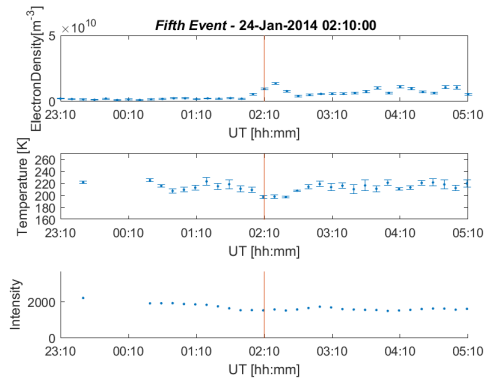
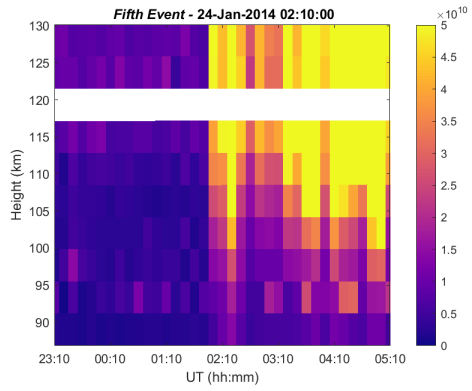


Figure 1. The upper panel shows the electron density as a function of altitude and time for the manda experiment at 16:00–22:00 UT on 6 January 2019. Particle precipitation event starts at 19:50 UT (vertical red line). The data are post-integrated to 0.6 km resolution at 80 km height to 3–4 km resolution at 100 km height and 60 s time resolution. The middle panel contains OH temperature data and the bottom panel displays the evolution of the relative band brightness, both in 30-minute averages at every 10 minute.





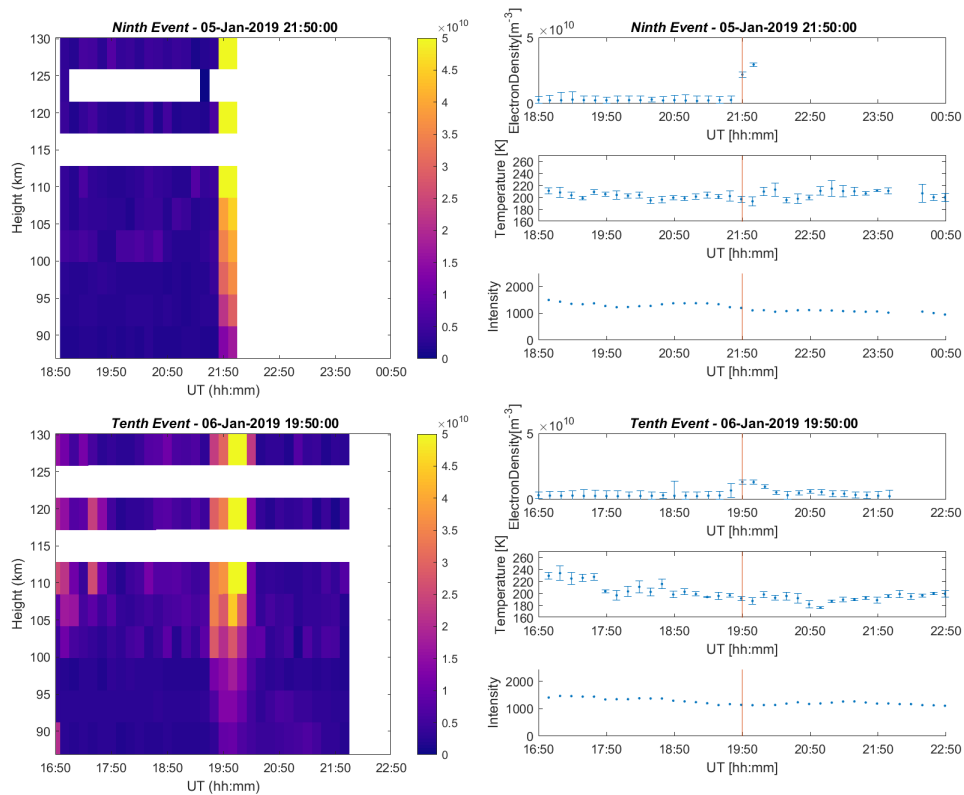


Figure 2. The left column shows the averaged electron density as a function of altitude and time. The right column illustrates the electron density time evolution at the height range where the electron density enhancement was detected. The temporal evolution of the airglow temperature (middle panel) and the relative OH(6–2) band intensity in arbitrary units (bottom panel) are also included. The temperature and intensity measurements are shown at the end of their half-hour integration time. All time axes are given from 3 hours before to 3 hours after the EPP onset, which takes place in the middle of the plot. The white gaps in the electron density plots indicate missing data.

Figure 2 displays all the individual EPP events for clarity. The left panels present electron density measurements as a function of time and altitude, for a 6 hour interval centered at the EPP onset. The right column includes the temporal evolution of the D region electron density (top panel), the airglow temperature (middle panel) and the relative OH(6–2) band intensity (bottom panel). In the line plots the electron densities are from the lowest height range where the increase by a factor 4 was detected. Brief descriptions of each event are given in the following paragraphs.

The first event commences at 23:30 UT on 29 December 2007 and is detected in the altitude range of 91–94 km. The electron density at the EPP event start time is $1.0 \times 10^{10} \text{ m}^{-3}$. The electron precipitation lasts for about 30 min. The mesopause temperature decreases by 40 K (from 225 to 185 K) over the EPP onset time, and recovers within an hour after the onset. The relative OH(6–2) band intensity is 148 before the event and only slightly diminishes to 133 over the EPP onset.

The second event starts at 02:50 UT on 28 February 2008. The electron density enhancement is detected in the height range of 91–94 km with an onset time value of $1.2 \times 10^{10} \text{ m}^{-3}$. The precipitation lasts for about 40 min and is followed by another

180 increase lasting for about 50 min (from 04:00 until 04:50 UT). An airglow temperature decrease of 13 K (from 215 K to 202 K) is observed at the EPP onset time. The decrease is large but just within the standard deviation error bars. ~~There is only one temperature data point available after the event onset, suggesting an increase of 10 K an hour after the EPP onset.~~ The relative OH(6–2) band intensity decreases gradually from 2 hours before the event until the event onset time. Thus, during this event the intensity behavior is much smoother than that of the temperature. Little or no correlation is seen between the two parameters.

185 ~~The *fourth third* event~~ starts at 21:50 UT on 6 December 2013. It is detected in the altitude range of 87–90 km with an electron density value of $9.9 \times 10^9 \text{ m}^{-3}$. The soft precipitation lasts for around 30 minutes. The temperature decreases by 23 K (from 219 to 196 K) over the event onset time. Both temperature and electron density values recover within ~~30 minutes an hour.~~ The relative band intensity peaks at 1320 half an hour before the onset, decreases to 1011 at the onset and minimizes at 864 after the electron density maximum. A positive correlation between the temperature and band intensity is found in this
190 case.

~~The *fourth event*~~ starts at 15:20 UT on 21 January 2014, detected in the altitude range of 87–90 km with an electron density value of $1.7 \times 10^{10} \text{ m}^{-3}$. The precipitation continues for about an hour. The temperature falls by 10 K (from 222 to 212 K) over the onset time. The electron density falls within the next half hour but increases again to $1.6 \times 10^{10} \text{ m}^{-3}$ about 40 minutes after the onset. The temperature values increase to its background level at the time the electron density peaks a second time. The
195 relative band intensity is stable. However the slight intensity variations coincide with the peaks and drops in the temperature evolution.

~~The *fifth event*~~ starts at 02:10 UT on 24 January 2014 at an altitude range of 87–90 km. The electron density at the precipitation onset is $9.5 \times 10^9 \text{ m}^{-3}$, and stays slightly elevated for about two hours after the initial enhancement, which only lasts for about 30 minutes. The mesopause temperature undergoes a decrease of about 12 K, from 210 K prior to the event to
200 198 K after the EPP onset. The temperature recovery follows that of the initial enhancement in electron density. The OH(6–2) band intensity decreases from 1890 to 1551 already an hour prior to the EPP onset. Similar to the temperature evolution, the emission intensity recovers within half an hour after the onset. There is a mild positive correlation between the temperature and band intensity values.

~~The *sixth event*~~ commences at 15:20 UT on 24 January 2014 in the altitude range of 87–90 km. The electron density enhancement is seen in a single profile only (10 min lifetime), with the value of $1.5 \times 10^{10} \text{ m}^{-3}$. The mesopause temperature undergoes mild fluctuations, but all changes are well within the errors and thus, this event is classified as stable. The relative OH band intensity strongly increases (from 460 to 1079) during half an hour before the onset. After the event onset a more steady and gentle increase in the emission intensity is seen. A more persistent mesospheric electron density enhancement below
205 95 km may refer to an evolution of sporadic E layer which can affect the temperature evolution. Furthermore, the short lifetime
210 of the electron density enhancement is a good candidate to explain the temperature stability.

~~The *seventh event*~~ begins at 02:40 UT on 25 January 2014. It is detected at an altitude range of 87–90 km with an electron density value of $2.6 \times 10^{10} \text{ m}^{-3}$. The electron density enhancement is strong for about 20 min and remains at an elevated level for the next couple of hours. The mesopause temperature stays stable over the event onset. The OH band intensity values also keep constant with respect to the intensities an hour before the EPP event.

215 *The eighth event* is detected at 19:50 on 6 February 2016 in the altitude range of 87–90 km with an electron density value of $5.2 \times 10^9 \text{ m}^{-3}$. The light precipitation lasts for 50 minutes. The mesopause temperature decreases by 13 K from pre-EPP level 195 K to post-EPP level 182 K. Comparing the same time steps the emission intensity decreases from 1164 to 911 in correlation with the temperature.

220 *The ninth event* commences at 21:50 on 5 January 2019 at the altitude of 91–94 km with an electron density value of $2.2 \times 10^{10} \text{ m}^{-3}$. The temperature increase at the EPP event onset is within the standard deviation error bars and therefore classified as stable. The electron density measurements are only available until ten minutes after the onset time, but display a steep increase until then. The temperature decreases and increases around the event onset are only minor, so the event is classified as stable. The relative band intensity is 1372 half an hour before the onset, 1201 at the onset time and 1058 half an hour after onset, which is a more systematic decrease than what is seen in the variable temperature.

225 *The ~~eighth~~ tenth event* starts at 19:50 UT on 6 January 2019 and is detected in the altitude range of 91–94 km. The electron density at the EPP onset is $1.3 \times 10^{10} \text{ m}^{-3}$, and the enhancement lasts for about 30 minutes. The mesopause temperature does not decrease when comparing the level before the precipitation to that when the electron density is first enhanced. ~~Nevertheless, there is a decrease of 21 K (from 198 K to 177 K) at about an hour past the event onset.~~ The relative OH(6–2) band intensity at the event onset is 54 units higher than the level before the event onset time, but stays otherwise constant throughout the
230 analysis window.

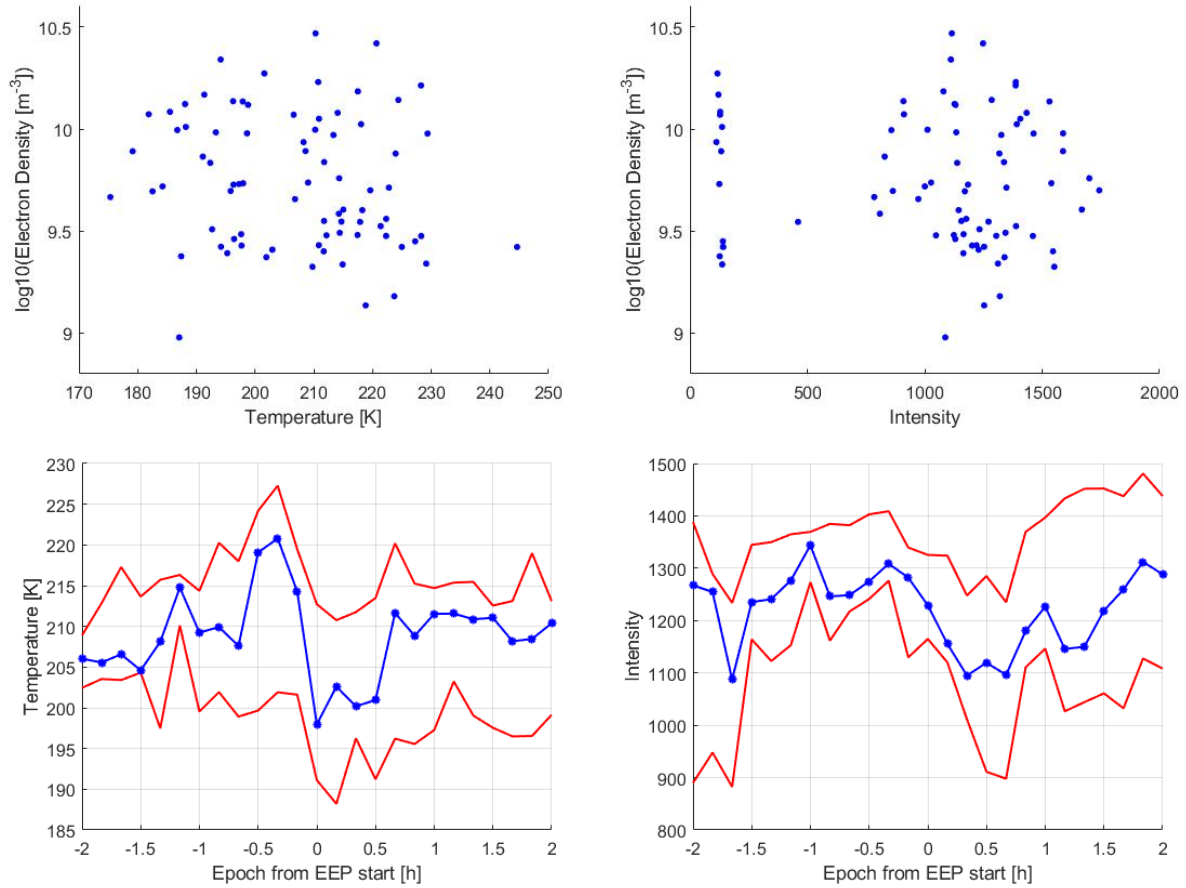


Figure 3. This figure illustrates the average temperature and intensity response to the EPP onset. The upper left (right) panel shows a scatter plot of the electron density and the airglow temperature (intensity) values, including data points from half an hour before to one hour after the EPP event. The superposed epoch of the airglow temperature in the lower left panel (airglow intensity in the lower right panel) includes the 25% (lower red line), 50% (blue) and 75% (upper red line) percentiles of the temperature for all eight ten events. The lower percentile for intensity 35%. The zero epoch time corresponds to the EPP onset. The measurements are chosen closest to the respective epoch time and averaged. Each 30 min epoch time bin contains 3–7 6–10 temperature (intensity) values.

An overall temperature response to the EPP onsets is shown in Figure 3 by a scatter plot (upper left panel) and superposed epoch analysis (lower left panel). The scatter plot includes all simultaneous temperature and electron density value pairs from 30 minutes before to 60 minutes after the EPP onset. The result is a mild anti-correlation between the electron density and the airglow temperature with a large range of variation. The average temporal evolution of the temperature response is seen in the superposed epoch analysis from 2 hours before to 2 hours after the precipitation onset (bottom left). The zero epoch time (EPP onset) shows the lowest temperature both in the median (blue), upper and the lower percentile (red) curves. This immediate temperature decrease is of the order of 20 degrees and recovers within half an hour after the EPP onset. Similarly, the scatter plot of electron density and the relative airglow intensity (top right) suggests a mild negative correlation at brightness values around and larger than 1000 counts. The median, upper and lower percentile of the airglow intensity (bottom right) shows about 15% decrease at zero epoch time, which recovers in tandem with the median temperature.

5 Discussion

We have found and analyzed ten electron precipitation events which reached the mesopause and had a good coverage of co-located OH airglow temperature data. Table 1 shows that 6 out of 8 EPP events analyzed in this study were accompanied by a decrease in the mesopause temperature by 10–40 K at the EPP onset. The pre-EPP temperature level (temperature values 10–20 minutes before the event) varied between 196–194 and 234–229 K, and the temperature decreased to the range of 222–214–211 K.

The winter mesopause is characterized by a large temperature variability (of the order of 10 K, Suzuki et al. (2010b)) due to gravity wave propagation. It is thus understandable that there is no consensus of the temperature response to the energetic particle precipitation when any minor change is likely to be lost in the highly variable background conditions. The temperature responses found in this study, however, were often larger than 10 degrees. The short lifetime (<60 minutes) of the observed temperature responses does not allow this signature to be detected in analysis utilizing hourly or daily averaged temperature data. For instance, the fast temperature decrease and equally quick recovery shown by the superposed epoch analysis (bottom left panel of Figure 3) would not be seen as a change in hourly or daily averaged epoch.

The first event (top panel of Figure 2) shows a strong decrease in the mesopause temperature at the time of the EPP onset. Similarly, in the third event and fourth event the eighth event quiet ionospheric conditions (low electron density) are seen prior to the EPP onset, and the connection between the electron density enhancements and the temperature changes is clear. This is a typical behavior in our set of events. It is further demonstrated by the anti-correlation between the airglow temperature and the electron density seen in the top panel of Figure 3.

In the second, fourth and fifth the short-lasting electron density enhancements are followed by longer lasting but gently elevated levels of electron densities. In all these cases the electron fluxes reaching the E region heights (above 100 km) are high for a couple of hours after the EPP event, but only at the very beginning of the precipitation event did they reach the altitudes below 100 km. Consequently, the temperature behaviour is smooth and steady apart from the short-term change around the

EPP onset. *The second event shows the same characteristics of an apparent decrease. However, the decrease is of the order of the standard deviation and thus includes a large uncertainty.*

265 Our *sixth, seventh, ninth and ~~eighth event~~ tenth event* were classified as stable in terms of the mesospheric temperature response. The electron density increase in *sixth event* has the shortest lifetime of all our events, as it is seen in one 10-min profile only. *Similarly, the tenth event is short-lived.* The lifetime of the electron bombardment may thus be the key factor determining whether a measurable neutral temperature response is seen.

270 A statistical study on high-latitude OH airglow temperatures and emission intensities by Shepherd et al. (2007) shows a strong positive correlation between the two parameters in the time scales from hours to seasons. This is explained by vertical motion of the airglow layer driven by atmospheric dynamics. For instance, as an airglow layer undergoes downward motion the adiabatic heating increases its temperature. The lower peak emission height coincides with higher mixing ratio of oxygen and therefore, enhances the production of the excited OH. The temperature changes observed in our study take place in shorter time scales. The correlation between the OH(6–2) temperature and the relative band intensity of 30-minute averaged data can be
275 visually inspected in Figure 2. While a positive correlation can be seen between the two parameters in case of the *fourth third, fifth and eighth* event, only mild anti-correlation across the entire event set was found (shown in Figure 3). As the scatter plots include data points from 30 minutes before to 60 minutes after the onset time, the lack of scatter correlation suggests that there is no larger-scale or periodic coherent behaviour between temperature and brightness within the examined time period. The synchronous decrease in temperature and brightness seen in the epoch curves is a short-term feature, which does not dominate
280 the scatter. A periodic out-of-phase relationship between temperature and brightness, which has been observed for non-EPP conditions Suzuki et al. (2010a) would result in low correlation but would not explain the synchronous decrease at onset.

An increase in the mesospheric temperature during particle precipitation would agree with the Joule heating effect suggested by earlier studies (Nesse Tyssøy et al., 2010). In fact, a temperature increase of about 10 K was observed in the study by Suzuki et al. (2010b). In our study, however, the mesopause temperature responded to the particle impact with a decrease of
285 about 20 K in *6 out of 10 events*. A way to explain the temperature change Suzuki et al. (2010b) discussed was that the EPP ionisation changes the mesospheric chemical composition by decreasing the population of excited OH at the top of the layer. As a consequence, the peak height of the airglow changes and the temperatures are *probed at weighted by* lower altitudes than before. The energetic electron impact can dissociate oxygen and ozone molecules in the mesosphere (e.g. Turunen et al., 2016). When less O₃ is available, less excited OH molecules are produced as ozone is a key ingredient in the production of excited
290 hydroxyl:



where v' corresponds to the upper vibrational level of the OH molecule, which in our case is 6. The dissociation of molecular oxygen and ozone by energetic electrons can therefore lead to a decrease in the emission of the OH airglow. The fitted rotational OH temperature corresponds to the height of the airglow layer. The peak is assumed to be at about 87 km. If, however, the
295 production of excited OH is temporarily prohibited at the top part of the airglow layer, the temperature will then represent the layer, which is now centered at lower heights. Depending on the local gradient in the mesospheric temperature profile, this

may lead to increased, decreased or unchanged temperature value. In this scenario, the relative OH(6–2) band intensity would decrease as the airglow layer becomes thinner, which is true for most of the events analyzed in this study. In particular at the top of the mesosphere the temperature can vary on the order of 10 K over a height range of a few kilometers. Mesospheric winter time temperatures are also often constant over a large range of heights, which results in no change in the temperature even if the OH layer height changes.

According to the superposed epoch behaviour in Figure 3, a typical temperature decrease at the event onset is about 20 K, while that for the relative band brightness is about 20–15%. On a Gaussian airglow profile (as for instance depicted by Suzuki et al. (2010b) in their Figure 4) an intensity reduction of 20–15% would correspond to thinning of the airglow layer by about 2 km, and a gradient in the temperature profile of about 10 K/km. While no measured mesospheric temperature profiles were available during the events analysed here, browsing polar night temperature measurements by SABER/TIMED spacecraft showed that a downward temperature decrease by 5–10 K/km at the airglow altitude is not uncommon. However, the first event with a temperature decrease of 50–40 K is not realistically explained by the depletion of OH alone.

Our results together with the previous results by Suzuki et al. (2010b) present an inconsistent temperature response to EPP. Therefore, a larger number of events should be collected and examined to ~~conclude if the OH airglow layer favors a height region with a positive temperature gradient upwards~~ investigate which precipitation parameters and background ionospheric conditions play key roles in the final outcome. Furthermore, an immediate temperature response and its fast recovery suggests that the longer-term and larger-scale heat balance in the mesosphere is little affected by EPP, unless the actual precipitation has a substantial lifetime (hours to days).

315 6 Conclusions

A total of 10220 hours of electron density measurements were browsed in the search of enhancements due to energetic electron precipitation (EPP) events with simultaneous temperature calculations from OH airglow measurements. A total of eight ten events of electron density enhancements were found and analyzed in this study. Although the number of events is not statistically sound, the results are systematically pointing to a short-term EPP effect on neutral temperature based on co-located measurements and in particular, direct electron precipitation measurements. We searched for any coherent behaviour between the electron density enhancements at the D region heights and the mesopause temperature. The response of the mesopause temperature on the EPP energy deposition is predominately (6 out of 8–10 events) an immediate decrease of 10–50–40 K, which recovers within less than 60 minutes after the EPP onset. In case of 4 events the temperature change was only a few decrease and well within the averaging uncertainty. Our findings together with a temperature increase in a previous study suggests that an EPP ionisation may decrease the production of the excited OH at the top of the airglow layer. As a consequence, the airglow layer becomes thinner, the peak height is reduced and the airglow temperatures correspond to lower altitudes. Investigating the change in the relative OH(6–2) band intensity shows a decrease during the majority of our EPP events, thus supporting the thinning scenario as a valid mechanism for changing the measured temperature. Furthermore, the relative OH brightness values are only poorly correlated with the temperatures in the time scales of a few hours, which is not in agreement with purely dynamical

330 cally driven temperature changes. [Four events showing no change in temperature may indicate that the mesospheric temperature stays constant over a larger range of heights.](#) Given the short-lived characteristic of atmospheric temperature change, EPP may not have climate effects except for long-lasting events.

Data availability. The temperature data are available as quicklooks plots online at kho.unis.no. The EISCAT Svalbard Radar data have been downloaded from <https://eiscat.se> and are the intellectual property of the EISCAT Scientific Association. The EISCAT raw data files are
335 analyzed by using the Grand Unified Incoherent Scatter Design and Analysis Package (GUISDAP) Lehtinen and Huuskonen (1996).

Author contributions. Florine Enengl carried out the analysis of the data and the writing of the paper. Noora Partamies proposed the idea of the study, fitted and pre-analyzed the airglow temperature data, shared her expertise and together with Nickolay Ivchenko took part in the discussions, interpretations, planning and structure of the work. Lisa Baddeley advised and helped describing and analysing the EISCAT data. All co-authors helped in the writing process with comments, suggestions and edits on the paper.

340 *Competing interests.* No competing interests are present.

Disclaimer. The data and figures have been used in the MSc thesis by F. Enengl, available through <http://kth.diva-portal.org/>

Acknowledgements. The work by NP & LB is supported by the Research Council of Norway (NRC) under CoE contract 223252, and NP is further supported by the NRC contract 287427. The authors thank Fred Sigernes and Mikko Syrjäsuo for the maintenance of the OH airglow spectrometer. EISCAT is an international association supported by research organisations in China (CRIRP), Finland (SA), Japan (NIPR and
345 ISEE), Norway (NFR), Sweden (VR), and the United Kingdom (UKRI). The authors thank Ingemar Häggström for his assistance with the EISCAT data.

References

- Andrews, D. G.: An Introduction to Atmospheric Physics Second Edition, CAMBRIDGE UNIVERSITY PRESS, 2010.
- 350 Blelly, P. L., Alcayd , D., and van Eyken, A. P.: A new analysis method for determining polar ionosphere and upper atmosphere characteristics from ESR data: Illustration with IPY period, *Journal of Geophysical Research (Space Physics)*, 115, A09322, <https://doi.org/10.1029/2009JA014876>, 2010.
- Cho, Y. and Shepherd, G. G.: Correlation of airglow temperature and emission rate at Resolute Bay (74.68 N), over four winters (2001–2005), *Geophysical Research Letters*, 33, n/a–n/a, 2006.
- 355 Cresswell-Moorcock, K., Rodger, C. J., Kero, A., Collier, A. B., Clilverd, M. A., Haggstrom, I., and Pitkanen, T.: A reexamination of latitudinal limits of substorm-produced energetic electron precipitation, *Journal of Geophysical Research. Space Physics*, 118, 6694–6705, <https://doi.org/10.1002/jgra.50598>, 2013.
- Gavriljeva, G. and Ammosov, P.: Influence of geomagnetic activity on mesopause temperature over Yakutia, *Atmospheric Chemistry and Physics*, 18, 3363–3367, <https://doi.org/10.5194/acp-18-3363-2018>, 2018.
- 360 Holmen, S., Dyrland, M., and Sigernes, F.: Mesospheric temperatures derived from three decades of hydroxyl airglow measurements from Longyearbyen, Svalbard (78 N), *Acta Geophysica*, 62, 302–315, <https://doi.org/10.1029/2001JA009023>, 2014.
- Holmen, S. E., Dyrland, M., and Sigernes, F.: Mesospheric temperatures derived from three decades of hydroxyl airglow measurements from Longyearbyen, Svalbard (78N), *Acta Geophysica*, 62, <https://doi.org/10.2478/s11600-013-0159-4>, 2013.
- Lehtinen and Huuskonen: First experiences of full-profile analysis with GUIDAP, *Annales Geophysicae*, European Geosciences Union, pp. 1487–1495, <https://doi.org/10.1007/s00585-996-1487-3>, 1996.
- 365 Mulligan, F., E. Dyrland, M., F. S., and S. Deehr, C.: Inferring hydroxyl layer peak heights from ground-based measurements of OH(6–2) band integrated emission rate at Longyearbyen (78 N, 16 E), *Annales Geophysicae*, 27, <https://doi.org/10.5194/angeo-27-4197-2009>, 2009.
- Nesse Tyss y, H., Stadsnes, J., S rb , M., Mertens, C. J., and Evans, D. S.: Changes in upper mesospheric and lower thermospheric temperatures caused by energetic particle precipitation, *Journal of Geophysical Research: Space Physics*, 115, 370 <https://doi.org/10.1029/2010JA015427>, 2010.
- Rapp, M., Leitert, L., Latteck, R., Zecha, M., Hoffmann, P., H ffner, J., Hoppe, U., La Hoz, C., and Thrane, E. V.: Localized mesosphere-stratosphere-troposphere radar echoes from the E region at 69 N: Properties and physical mechanisms, *Journal of Geophysical Research: Space Physics*, 116, n/a–n/a, 2011.
- 375 Shepherd, G., Cho, Y.-M., and Liu, G.: Correlations of mesospheric variability and their relation to the large-scale circulation during polar winter, *Journal of Atmospheric and Solar-Terrestrial Physics*, 69, 2279–2291, <https://doi.org/10.1016/j.jastp.2007.06.007>, 2007.
- Sigernes, F., Shumilov, N., Deehr, C. S., Nielsen, K. P., Sven e, T., and Havnes, O.: Hydroxyl rotational temperature record from the auroral station in Adventdalen, Svalbard (78N, 15E), *Journal of Geophysical Research: Space Physics*, 108, <https://doi.org/10.1029/2001JA009023>, 2003.
- 380 Suzuki, H., Tomikawa, Y., Taguchi, M., Nakamura, T., and Tsutsumi, M.: Variations of OH rotational temperature over Syowa Station in the austral winter of 2008, *Earth, Planets and Space*, 62, 655–661, 2010a.
- Suzuki, H., Tsutsumi, M., Nakamura, T., and Taguchi, M.: The increase in OH rotational temperature during an active aurora event, *Annales Geophysicae*, 28, 705–710, <https://doi.org/10.5194/angeo-28-705-2010>, <https://www.ann-geophys.net/28/705/2010/>, 2010b.
- Tjulin, A.: EISCAT experiments, <https://www.eiscat.se/wp-content/uploads/2016/05/Experiments.pdf>, 2017.

- 385 Turunen, E., Kero, A., Verronen, P. T., Miyoshi, Y., Oyama, S.-I., and Saito, S.: Mesospheric ozone destruction by high-energy electron precipitation associated with pulsating aurora, *Journal of Geophysical Research: Atmospheres*, 121, 11,852–11,861, <https://doi.org/10.1002/2016JD025015>, <https://agupubs.onlinelibrary.wiley.com/doi/abs/10.1002/2016JD025015>, 2016.
- Wannberg, G., Wolf, I., Vanhainen, L. G., Koskenniemi, K., Röttger, J., Postila, M., Markkanen, J., Jacobsen, R., Stenberg, A., Larsen, R., Eliassen, S., Heck, S., and Huuskonen, A.: The EISCAT Svalbard radar: A case study in modern incoherent scatter radar system design, *Radio Science*, 32, 2283–2307, <https://doi.org/10.1029/97RS01803>, 1997.

Response to Referee 3

We want to thank Referee 3 for careful reading of the manuscript and thoughtful comments. Below are the point-by-point responses (blue) to each of the comments (black). The spectrometer data have been re-analyzed. The integration time remains 30 minutes, but the temperature points are generated every ten minutes. This allows us to see a more continuous (albeit smoothed) behaviour of the temperature. Nevertheless, the main results and key conclusions remain unchanged. Three more events could be included by further relaxing the data selections criteria, which is reflected by larger uncertainties displayed as error bars. One previously included had to be excluded due to too large uncertainties in the calculated temperature values. The re-analyzed events remained in the same temperature-change categories as before.

1. Some clarification/rewording needed in L4–5 (abstract) — it is explained later than you use all manda/ipy experiments between the start of the IPY and Feb 2019, but this sentence reads as if the experiment was run continuously between the IPY and Feb 2019.

The revised abstract says that we use all the available experiments from the IPY until February 2019.

2. In Table 1 perhaps display the quantitative magnitude of the change in temperature as well as the classification of increasing/decreasing/stable.

The table has been updated accordingly.

3. During discussion of 3rd event (L178–183) the author states: ‘The minimum temperature is measured at the time of the electron density maximum’ however in the corresponding plot of Figure 2 there is no temperature measurement coincident in time with the electron density peak (at ~22:50UT).

The event has now been excluded from the study as the uncertainties became too large.

4. Some clarification needed during discussion of the superposed epoch analysis (L213– 222). Are the OH temperatures/intensities averaged to produce the temperature/intensity values at the EPP onset time (e.g. Epoch 0) the measurements closest to the onset in time (as discussed earlier)? I understand this is implied when generating a superposed epoch analysis, but a statement that the measurements are never exactly aligned with epoch 0 or the EPP onset time would aid clarity.

The data averaging has now been changed so that a temperature point is generated every ten minutes, although we still integrate for 30 minutes. The value at Epoch 0 thus includes data collected during the previous half an hour. The averaging is clarified accordingly in the text.

5. Author states on L219–220 that ‘The upper percentile does not show a clear signature of a temperature decrease’ whereas the plot shows the upper red curve showing a similar decrease in temperature (at epoch 0) to the median and lower percentile curves. Some clarification needed. L217–218 also states that: ‘The zero epoch time (EPP onset) shows the lowest temperature both in the median (blue) and the lower percentile (lower red) curves.’ The temperature at zero epoch for the median curve, is not the lowest temperature seen within that curve, so some rewording needed, likely just to clarify that it is a local decrease seen at epoch 0, rather than a global minimum.

The plots have all been updated due to the re-analysis of the data and wording has been updated accordingly. Both percentiles show clear decreases around the onset times.

6. Author’s discussion regarding the potential OH temperature changes driven by large scale atmospheric dynamics (Paragraph containing L248–260) is valid and necessary in the discussion. However, the added lines from L255 onward discuss a scatter plot which is not presented in the article (scatter of OH-I vs OH-T), perhaps include this scatter plot in Figure 3? There is room in the top panel alongside the OH-I vs E-dens. scatter plot.

Good point. The scatter plot of airglow band brightness and electron density has been included in the new version of Figure 3, and for large intensity values it also shows a mild negative correlation.

7. Minor comments

The following comments have been implemented as suggested:

- 45 L2 (abstract): Sentence beginning “Recent results, however. . .” » “However, recent results are inconsistent, which leaves the mechanism and effects still unresolved”
L15 (abstract): “as opposed proxies” » “as opposed to proxies”
L58/59: “the temperature gradient in the mesosphere” » “the local temperature in the mesosphere” – clarification, as it is only dependent on the temperature gradient within the OH layer, not the entire mesosphere.
- 50 L60/61: “during the solar cycle 23 and 24” » “during solar cycles 23 and 24”
L77: “the spectrometer” » “spectrometer” – no need for ‘the’ since the spectrometer has not been formally introduced yet, just spectrometer measurements is fine
Figure 1: Caption, last sentence: “The vertical red lines in the mark the time. . .” » “The vertical red lines mark the time. . .” – no need for ‘in the’
- 55 L245: “Our sixth event and eight event was classified. . .” » “Our sixth event and eight event were classified. . .” – replace ‘was’ with ‘were’ since it is now plural (two events)
L284: Replace ‘height’ with ‘altitudes’

Response to Referee 4

We thank Referee 4 for reading and evaluating the manuscript. Below is our response (blue) to the presented comment (black).

- 5 *I feel that the measurements need to be of much better quality. A photometer using multiple filters to measure the rotational temperature from the ratio of two OH emissions would produce results with much improved precision.*

10 The instrumentation we have for the airglow is the spectrometer. It measures the OH spectrum, which is then used to fit the intensities of four emission line pairs to give the mesopause temperature. The method itself is robust, although there are other caveats in the data, as discussed in the paper. Comparing temperature values obtained from two different OH bands would be trickier, because they then originate from slightly different altitudes, which would impose further uncertainties in the interpretation.

15 So instead, the spectrometer data have been re-analyzed. The integration time remains 30 minutes, which is necessary to obtain good signal-to-noise ratio, but the temperature values are generated every ten minutes. This provides a more continuous (albeit smoother) behaviour of the temperature. Nevertheless, the main results and key conclusions remain unchanged, and the re-analyzed events remained in the same categories as before.